actuators

MDPI

Article

A Novel Caterpillar-Inspired Vascular Interventional Robot Navigated by Magnetic Sinusoidal Mechanism

Xinping Zhu, Hanwei Zhou, Xiaoxiao Zhu and Kundong Wang *

School of Electronic Information and Electrical Engineering, Shanghai JiaoTong University, Shanghai 200240, China; doctorzhu@sjtu.edu.cn (X.Z.); cyberman@sjtu.edu.cn (H.Z.); ttl@sjtu.edu.cn (X.Z.)
* Correspondence: kdwang@sjtu.edu.cn

Abstract: Magnetic soft continuum robots (MSCRs) hold significant potential in fulfilling the requirements of vascular interventional robots, enabling safe access to difficult-to-reach areas with enhanced active maneuverability, shape morphing capabilities, and stiffness variability. Their primary advantage lies in their tether-less actuation mechanism that can safely adapt to complex vessel structures. Existing commercial MSCRs primarily employ a magnetic-pull strategy, which suffers from insufficient driving force and a single actuation strategy, limiting their clinical applicability. Inspired by the inchworm crawling locomotion gait, we herein present a novel MSCR that integrates a magnetic sinusoidal actuation mechanism with adjustable frequency and kirigami structures. The developed MSCRs consist of two permanent magnets connected by a micro-spring, which is coated with a silicone membrane featuring a specific notch array. This design enables bio-inspired crawling with controllable velocity and active maneuverability. An analytical model of the magnetic torque and finite element analysis (FEA) simulations of the MSCRs has been constructed. Additionally, the prototype has been validated through two-dimensional in-vitro tracking experiments with actuation frequencies ranging from 1 to 10 Hz. Its stride efficiency has also been verified in a three-dimensional (3D) coronary artery phantom. Diametrically magnetized spherical chain tip enhances active steerability. Kirigami skin is coated over the novel guidewire and catheter, not only providing proximal anchorage for improved stride efficiency but also serving similar function as a cutting balloon. Under the actuation of an external magnetic field, the proposed MSCRs demonstrate the ability to traverse bifurcations and tortuous paths, indicating their potential for dexterous flexibility in pathological vessels.

Keywords: magnetic soft continuum robots (MSCRs); bio-inspired soft robotics; harmonic magnetic actuation; sinusoidal mechanism; crawling locomotion

check for updates

Citation: Zhu, X.; Zhou, H.; Zhu, X.; Wang, K. A Novel Caterpillar-Inspired Vascular Interventional Robot Navigated by Magnetic Sinusoidal Mechanism. *Actuators* **2024**, *13*, 412. https://doi.org/10.3390/act13100412

Academic Editors: Zhuming Bi and Giulia Scalet

Received: 27 August 2024
Revised: 9 October 2024
Accepted: 11 October 2024
Published: 13 October 2024

Copyright: © 2024 by the authors. Licensee MDPI, Basel, Switzerland. This article is an open access article distributed under the terms and conditions of the Creative Commons Attribution (CC BY) license (https://creativecommons.org/licenses/by/4.0/).

1. Introduction

Cardiovascular diseases (CVDs) such as stroke and cerebral thrombosis remain the leading cause of morbidity and mortality worldwide, representing a significant public health challenge. According to the World Health Organization (WHO), an estimated 17.9 million people die from CVDs each year, accounting for 32% of all global deaths [1]. Compared to conventional surgical procedures, minimally invasive interventional surgery offers several advantages, including reduced trauma, minimal pain, shorter recovery periods, a faster achievement of therapeutic effects, and higher success rates. A crucial component of such procedures is the guidewire and catheter, which are medical instruments typically guided manually or robotically through an incision to the pathological region of the vascular system using a combination of pushing, pulling, and twisting motions. Commercially available guidewires are designed with various shapeable distal tips (such as single inflexion, reversed inflexion, triple inflexion, double inflexion, and RH catheter), allowing for selection to suit different clinical scenarios. However, percutaneous coronary intervention (PCI) faces technical challenges related to errors in instrument selection and the

complexity of navigating tortuous vessels [2,3]. The deficiency in active maneuverability often necessitates multiple attempts for navigating through tortuous vessels, along with repeated X-ray fluoroscopy for detection. This can lead to fatigue and potential health concerns for the surgeon. Furthermore, the guidewire, which typically measures one meter in length, experiences its flexibility being influenced by distal friction and complex anatomical geometries (as depicted in Figure 1D), such as sharp turns, loops, and kinks. These factors increase the risk of tissue damage, including vessel perforation, vasospasm, and vessel rupture [4,5]. The absence of proximal support may result in buckling when the guidewire is pushed, as illustrated in Figure 1C. In bifurcation scenarios, the guidewire may buckle into the incorrect vessel (Figure 1E). Surface modifications, such as paint-coating or the incorporation of specific lubricant ingredients, represent a viable approach to prevent buckling and ensure smoother navigation within complex anatomical structures [6]. Alternatively, improving the rigidity of the guidewire could be considered. However, increased stiffness may indeed elevate the risk of tissue trauma and compromise the device's maneuverability in intricate anatomical environments.

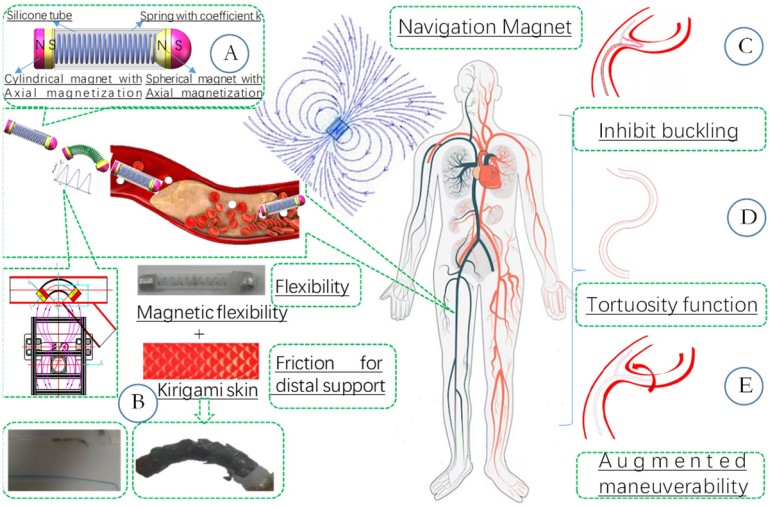


Figure 1. Harmonic MSCRs (magnetic soft continuum robots) feature a flexible magnetic pair tip that (**A**) realizes caterpillar-style locomotion gait while the multi-magnetic tip enhances flexibility and reduces bending stiffness for augmented maneuverability; (**B**) incorporates a kirigami surface, which provides proximal support; (**C**) can inhibit buckling; (**D**) can possess tortuosity, allowing for complex path navigation; (**E**) can realize augmented maneuverability.

Percutaneous coronary intervention (PCI) faces technical challenges related to errors in instrument selection and the complexity of navigating tortuous vessels [2,3]. The deficiency in active maneuverability often necessitates multiple attempts for navigating through tortuous vessels, along with repeated X-ray fluoroscopy for detection. This can lead to fatigue and potential health concerns for the surgeon.

Soft robots inspired by natural creatures possess the ability to adopt various shapes (shape morphing and stiffness variation) when interacting with pathological vessels. This has led to an ever-increasing interest from the robotics community in magnetic soft continuum robots (MSCRs) [7,8], owing to their intuitive nature, high dexterity, remote manipulation capabilities, and wireless actuation. There is a plethora of interventional instruments based on tendon/cable, multi-backbone, concentric tube, shape memory alloy (SMA), pneumatic/hydraulic driven, and other mechanisms [9]. However, the integration of these actuation models often leads to a cumbersome system accompanied by a complex control system. Magnetic actuation represents a cutting-edge, tether-free approach to energy transfer, eliminating the necessity for cumbersome on-board power-supply electronic modules. This technology facilitates the development of medical devices that meet rigorous sterility standards while remaining visually transparent to biomedical organs, as

it minimizes the obstruction of the device within the body during imaging and diagnostic procedures [10–12]. Probing proper actuation methodology and developing a simple manufacturing method are the main challenges of MSCRs [13]. Biomimetic design involves imitating or replicating biological motion patterns to enable adaptation to specific environments. In [14], a caterpillar-inspired soft-crawling robot actuated by programmable heat is proposed. Distributed and programmable heating and actuation using thermal-responsive materials have been tested as a valid method to realize bidirectional locomotion, similar to an inchworm. To provide proximal support, a helical protrusion [15] on the guidewire surface engages with the vessel wall and translates rotation into forward motion through contact friction force. However, the strategy of embedding rigid magnets for manipulation has been hindered by the damping effect on the pulling magnetic force or torque. Therefore, further research on actuation methods is needed to adapt to the vascular environment, especially in the fields of cardiac electrophysiology and ablation. Inspired by the locomotion gait of caterpillars and the skin characteristics of snakes [16–18], a novel actuation approach for magnetically driven soft catheters has been developed. This approach is based on the periodic interaction of magnetic and mechanical torques, where the vibration induced by an external periodic magnetic torque can overcome pushability limitations. By integrating this actuation methodology with magnetic steering, the necessary flexibility and active maneuverability are achieved to access hard-to-reach pathological targets within the vascular system. Additionally, kirigami art [19], an ancient Japanese paper-cutting technique, can realize 2D-to-3D shape transformations through shape morphing and stiffness variability. This is achieved by applying a specific array of precisely designed laser cuts to a planar plastic sheet, which is then adhered to the exterior of magnetic soft continuum robots (MSCRs). Periodic bending with an elongation of the magnetic tip stimulates the mechanical instability of the kirigami skin, accompanied by three-dimensional (3D) morphological changes. This mimics the way snakes actively tune their scales to control frictional properties. In [20], kirigami-style micro-needle aiming for maximizing local drug efficacy and minimizing potential systemic side effects has been researched. The highly directional 3D features of the kirigami skin endow the robot with adjustable frictional properties and provide anchoring points for proximal support.

These manipulators, which potentially possess unlimited degrees of freedom (DOFs), can enhance active maneuverability control through compliant bio-inspired motion. Consequently, they enable remote intervention by experienced surgeons via the Internet, making them a promising and potentially safe actuation method for vascular interventional surgery. This approach has the potential to improve surgical efficiency and allow for earlier disease control by the surgeon [21,22]. In addition, recent advancement in MEMS technology, computational methods, and AI have been leading to extensive research in sophisticated technology in micro-intravascular Intervention Surgical Robots, which lay the foundation and confidence for the development and biomedical applications of magnetic-driven guidewire.

Compared with existing works, the innovation of this study lies in the introduction of a novel magnetic actuation methodology, a kirigami-style skin, and a more intuitive navigation robot. This biomimetic actuation approach has not been previously utilized in soft robotics. This article is structured as follows: Section 2 presents the design and modeling of the harmonic magnetic catheterization robot, informed by technical and clinical needs. Section 3 describes the kirigami skin and its application for proximal support. Sections 4 and 5 provide a detailed description of the actuation strategy for the proposed MSCRs, followed by the presentation of experiments and results aimed at validating the proposed robot and actuation methodology. Finally, Sections 6 and 7 conclude the article with findings and future prospects.

2. Magnetic Catheterization Robot Design and Fabrication

Techniques for magnetic soft continuum robots (MSCRs) typically encompass four key sections: design, actuation, modeling, and control. Force modeling resulting from the magnetic field serves as a prerequisite for the detailed design of MSCRs. In this

context, we discuss the technical modules of the proposed vascular interventional robot, specifically focusing on the spherical magnetic chain for active maneuverability, the bio-inspired crawling mechanism, the kirigami skin for proximal support, and the actuation mechanisms for MSCRs.

2.1. Deflection Model for the Proposed Vascular Guidewire

A diametrically magnetized spherical chain structure with a radius of a can be utilized as the head of a guidewire, serving as an active maneuverability mechanism for magnetic guidance. This configuration enables large deflections and active steerability, facilitating navigation in tortuous and pathological vascular environments [23,24], as depicted in Figure 2.

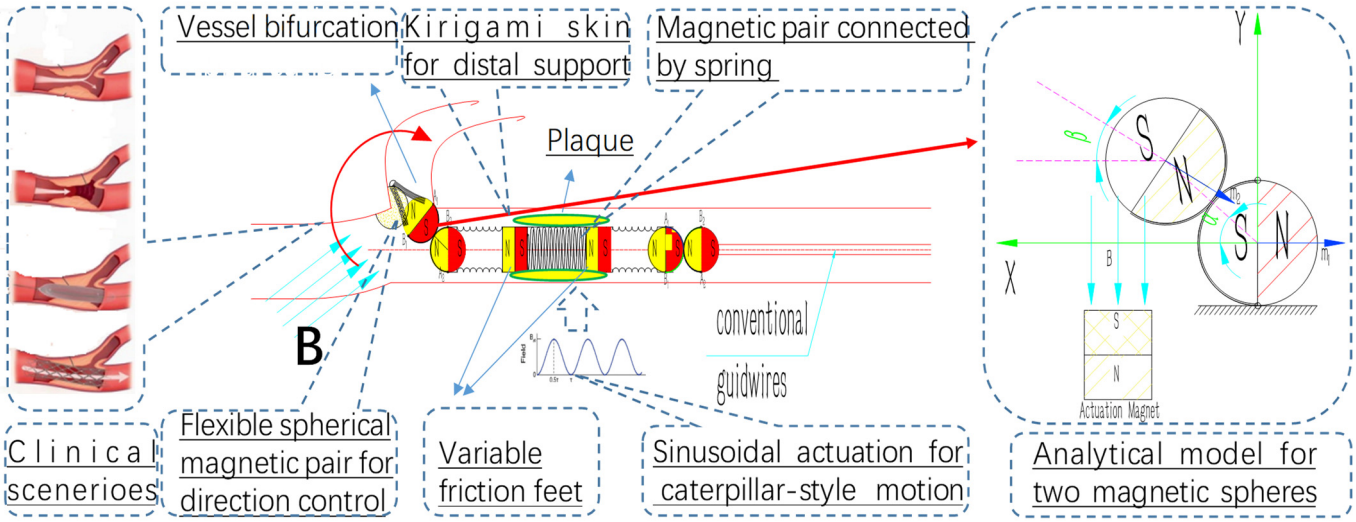


Figure 2. Illustration of a catheterization robot featuring a head equipped with magnetic spherical chains, a caterpillar-style body capable of inducing harmonic responses through a magnetic sinusoidal mechanism, and a tail also incorporating magnetic spherical chains that allow for the adjustment of the robot's deformation style.

A quantitative analysis of a simplified system comprising two spherical magnets in a two-dimensional (2D) plane is presented in Figure 2, with the establishment of a coordinate system illustrated to the right of the figure. An analytical model is formulated for two magnetic spheres interconnected by a micro-tendon, where the first sphere is fixed in position and aligned with the x-axis. The center point of the second sphere is free to traverse a circular path at an angle α relative to the first sphere and also to rotate around its own axis by an angle β. The navigation magnetic field, denoted as B, is oriented in the direction opposite to the positive y-axis.

$$\begin{aligned} \vec{\mathrm{r}} &= D(\vec{i}\cos\alpha + \vec{j}\sin\alpha) \\ \vec{m_1} &= |m_1|\vec{i} \\ \vec{m_2} &= |m_2|(\vec{i}\cos\beta + \vec{j}\sin\beta) \end{aligned} \tag{1}$$

$$U = \frac{\mu_0}{4\pi r^3}[\vec{m_1}\cdot\vec{m_2} - 3(\vec{m_1}\cdot\vec{r_{12}})(\vec{m_2}\cdot\vec{r_{12}})] \tag{2}$$

where μ_0 is the magnetic permeability of free space. Combining the above equations, Formula (2) tells us the energy of the second sphere m_2, and, due to the dipole–dipole interaction with the first sphere, m_1 can be simplified to the following equation.

$$U_{12} = \frac{\mu_0 \mathrm{m}_1 m_2}{4\pi D^3}[\cos\beta - 3\cos\alpha\cos(\alpha-\beta)] \tag{3}$$

As the potential energy derived from the external actuation magnetic field, B could be calculated by the following formula:

$$U = -m \cdot B \tag{4}$$

If the two spheres are placed in a uniform magnetic field at right angles to the x-axis and the first sphere m_1 is fixed in space, sphere m_2's potential energy is given in following equation.

$$U_{n2} = -m_2 B \sin\beta \tag{5}$$

Finding the partial derivative of total potential energy with respect to α, β is as follows:

$$\frac{\partial U}{\partial \alpha} = \frac{3\mu_0 m^2}{4\pi D^3} \sin(2\alpha - \beta) \tag{6}$$

$$\frac{\partial U}{\partial \beta} = \frac{\mu_0 m^2}{8\pi D^3} \sin\beta - \frac{3\mu_0 m^2}{8\pi D^3} \sin(2\alpha - \beta) - \mathrm{mBcos}\beta \tag{7}$$

Then, if we set

$$\frac{\partial U}{\partial \alpha} = 0, \; and \; \frac{\partial U}{\partial \beta} = 0$$

then

$$\beta = 2\alpha, \beta = \arctan(\frac{8\pi D^3}{\mu_0 m} B)$$

In the context of bifurcation procedures, the surgeon can adjust the orientation of the guidewire by precisely manipulating an external actuation magnetic device, leveraging real-time fluoroscopic imaging for guidance. This real-time adjustment capability enables the surgeon to mitigate errors in assessing the pathological vessel anatomy, ensuring a more accurate and safe navigation of the guidewire during the procedure.

2.2. Bio-Inspired Crawling Mechanism of Inchworm and Magnetic Sinusoidal Actuation Mechanism

A caterpillar-inspired interventional robot can dynamically respond to its environment by adopting a compliant locomotion gait capable of crawling. This robot has the potential to mitigate damage from contact and adapt to complex structures within the vasculature. Highly stretchable and morphable structures accompanied by friction variance is the basic element for crawling gait, named friction-attached locomotion. In this section, we propose modeling the crawling gait and actuation mechanism of the robot through the periodic activation of magnetic torque applied to its head and tail.

2.2.1. Bio-Inspired Crawling Mechanism of Inchworm

Crawling is a fundamental terrestrial locomotion mode [25], where caterpillars utilize their muscles in various combinations to periodically anchor their front and posterior legs. This results in an alternating pattern of a "semi-circular" configuration and a linear shape, named as the anchor push–anchor pull locomotion strategy, which facilitates effective discrete steps forward. This mode of movement, reminiscent of an inchworm's apparent "measuring" of distance, as suggested by its name, enables adaptability to complex three-dimensional environments (as depicted in Figure 3a). The legs at two ends create two states: high–low friction variation for locomotion and function as actuators. For linear crawling, the actuation of the legs and contraction of the muscle fibers are usually symmetric.

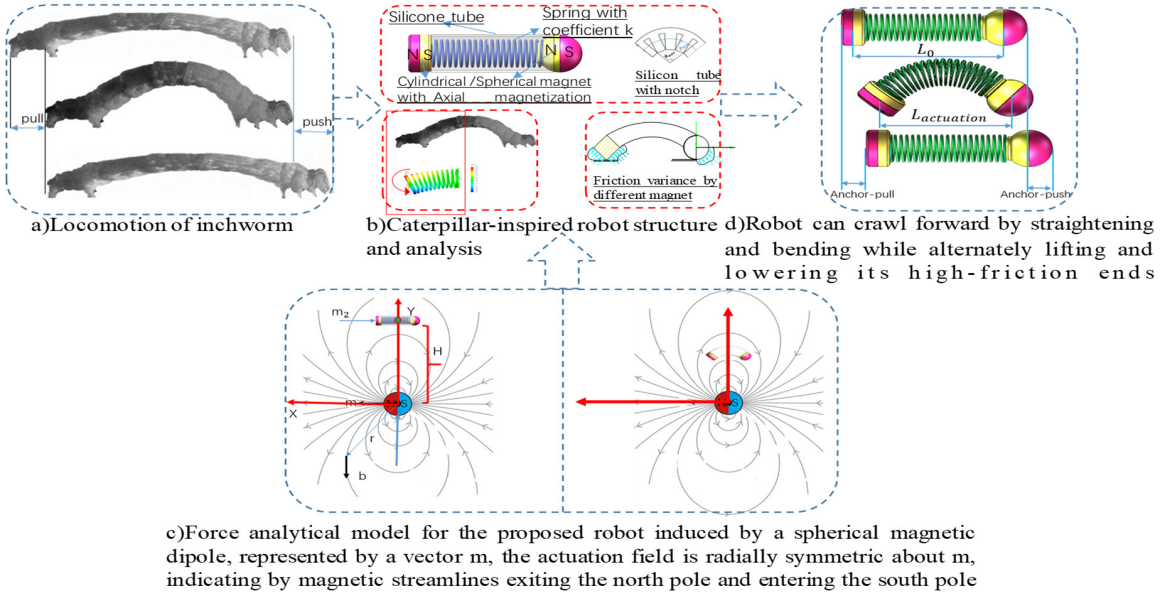


Figure 3. Caterpillar-inspired robot design for anchor push–anchor pull locomotion gait and calculation model for magnetic bending torque.

The locomotion gait of the inchworm serves as a source of inspiration for the design of our micro-robot, wherein the maintenance of a stable supporting point is achieved exclusively through the utilization of two distinct ends, as opposed to relying on the entire body structure. The detailed configuration of this innovative micro-robot is comprehensively depicted in Figure 3b, a system comprising two interconnected micro-magnets, with a spring serving as the intermediate linkage mechanism. The magnetic wrench $W = [F, \tau]^T, F \in R^3, \tau \in R^3$ for two magnets can be characterized by the interaction between their magnetic moments. When a micro-permanent magnet with moment m is exposed to an applied field B, it rotates and translates to minimize potential energy. The torque τ is the cross-product of the dipole moment and the actuation field, aligning the dipole with the field. The force on the dipole at location P_j due to the field gradient is described in equations [26], with parameters designed based on the inchworm locomotion mechanism.

$$\vec{F} = \left(\vec{m} \cdot \nabla\right)\vec{B} \qquad \vec{\tau} = \vec{m} \times \vec{B} \tag{8}$$

The magnetic field at position r due to an actuation spherical magnet with moment m is given by the following formula:

$$\vec{\mathrm{B}}(r, m) = \left(\frac{\mu_0}{4\pi\|r\|^3}\left(3\hat{r}\hat{r}^T - I\right)\right)\vec{m} \tag{9}$$

$\hat{r}$ is the unit vector for the position r:

$$\hat{r} = \frac{1}{\sqrt{\frac{1}{4}L^2 + H^2}}\begin{pmatrix}\frac{1}{2}L & H & 0\end{pmatrix}^T \tag{10}$$

Formula (9) tells us that the actuation magnetic field at the location of left PM is as follows:

$$\vec{B} = \begin{pmatrix}\frac{3}{4}L^2 - 1 & \frac{3}{2}HL & 0 \\ \frac{3}{2}HL & 3H^2 - 1 & 0 \\ 0 & 0 & -1\end{pmatrix}\begin{pmatrix}1 \\ 0 \\ 0\end{pmatrix}K = \begin{pmatrix}\frac{3}{4}L^2 - 1 \\ \frac{3}{2}HL \\ 0\end{pmatrix}K \tag{11}$$

where $K = \frac{1}{\frac{1}{4}L^2+H^2} \cdot \frac{\mu_0}{4\pi\|H\|^3}\|m_1\|$ and $H = L_0 - L_1 - R\sin(\omega t + \phi)$.

R is the length of the crank, ω is the rotational angular velocity, and Φ is the initial angular of the crank. The actuation torque on the left magnet is determined using Equation (8), which incorporates the left-multiplying a screw matrix to compute the cross-product as illustrated in the following equations.

$$\vec{c} = \vec{a} \times \vec{b}, then : \vec{c} = \hat{a}\vec{b} = \begin{bmatrix} 0 & -a_z & a_y \\ a_z & 0 & -a_x \\ -a_y & a_x & 0 \end{bmatrix} \begin{bmatrix} b_x \\ b_y \\ b_z \end{bmatrix}$$

In such applications, the magnetic soft continuum robots (MSCRs) actuated by magnetic fields are often positioned at distances significantly exceeding their own body lengths from the navigation magnetic equipment that generates the controlled magnetic field. The hypothesis that the magnetic field at the robot's center of mass is sufficient to accurately model the resulting force and torque can simplify the calculation model, potentially facilitating real-time control. The torque actuated on the internal embedded permanent magnet, based on Equation (8), can be expressed by the following equation.

$$\tau_z = -\frac{3}{2} HLK|m_2|$$

As illustrated in Figure 4, the same mechanical structure, when equipped with different magnet magnetization configurations (axial and diametrical magnetization), exhibits a more reasonable actuation torque, which is detailed in the following sections. The magnetic torque attempts to align the dipole with the actuation field, as quantified by Equation (8). Specifically, the bending torque for axial magnetization is calculated as follows:

$$\left|\vec{\tau}_1\right| = \left|\vec{m}\right| \cdot \left|\vec{B}\right| \sin\theta$$

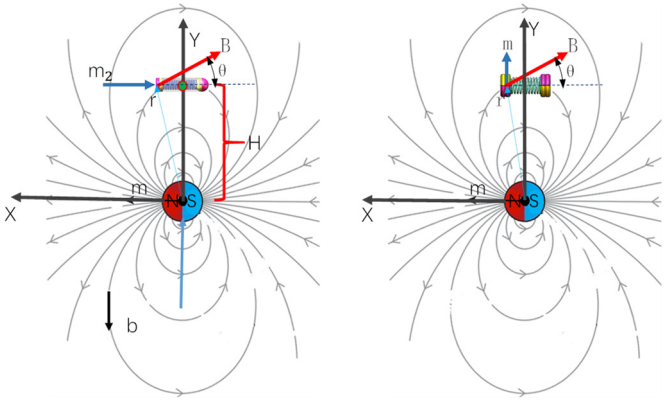


Figure 4. Bending torque comparative analysis for axial magnetization and diametrical magnetization.

In the case of diametrical magnetization combinations, the angle between the actuation field and the dipole moment is denoted as $\frac{\pi}{2} - \theta$, and the resulting bending torque is given by the following:

$$\left|\vec{\tau}_2\right| = \left|\vec{m}\right| \cdot \left|\vec{B}\right| \left|\sin\left(\frac{\pi}{2} - \theta\right)\right| = \left|\vec{m}\right| \cdot \left|\vec{B}\right| \cos\theta$$

It is evident that $\cos\theta \geq \sin\theta$, when $\theta \in (0, 45]$. Diametrical magnetization is more suitable for the proposed MSCRs, as it results in a larger actuation torque. Furthermore, combining diametrical magnetization with the same actuation methodology can increase the bending moment, thereby augmenting stride efficiency.

Friction asymmetry, with low forward friction for directionality and high friction at the endpoint for anchoring, drives crawling locomotion. Micro-magnets of varying geometries (cylindrical and spherical) are designed to induce this asymmetry. Additionally, a notched

array enhances bending flexibility, referred to as spring-tube linkage. The micro-spring linkage has been validated through FEA analysis.

2.2.2. Magnetic Sinusoidal Actuation Mechanism

Harmonic response analysis is conventionally used to simulate how a structure will respond to sinusoidal repeating dynamic loading. However, a vascular system, comprising a complex network of blood vessels that transport blood throughout the body, exhibits time-varying behavior due to the dynamic interplay of various physiological processes. Intrigued by the research on Resonant Magnetic Actuators reported in [27], a uniformly magnetized sphere with radius 50 mm and magnetic field B = 4000 Gs is designed to actuate the bio-inspired robot. Manufacturing a spherical magnet is a complex and costly process; thus, an array of cylindrical magnets can be used as an alternative to approximate the behavior of an actual spherical magnet (as depicted in Figure 5a). The actuation principle is based on harnessing the interactive torque between IPM and EPM in a periodic magnetic field to drive MSCRs to resonance. In a sinusoidal mechanism (its schematic diagram is illustrated in Figure 5b), the motion of its components follows a sinusoidal path or profile. This means that the displacement, velocity, or acceleration of these components varies sinusoidally over time.

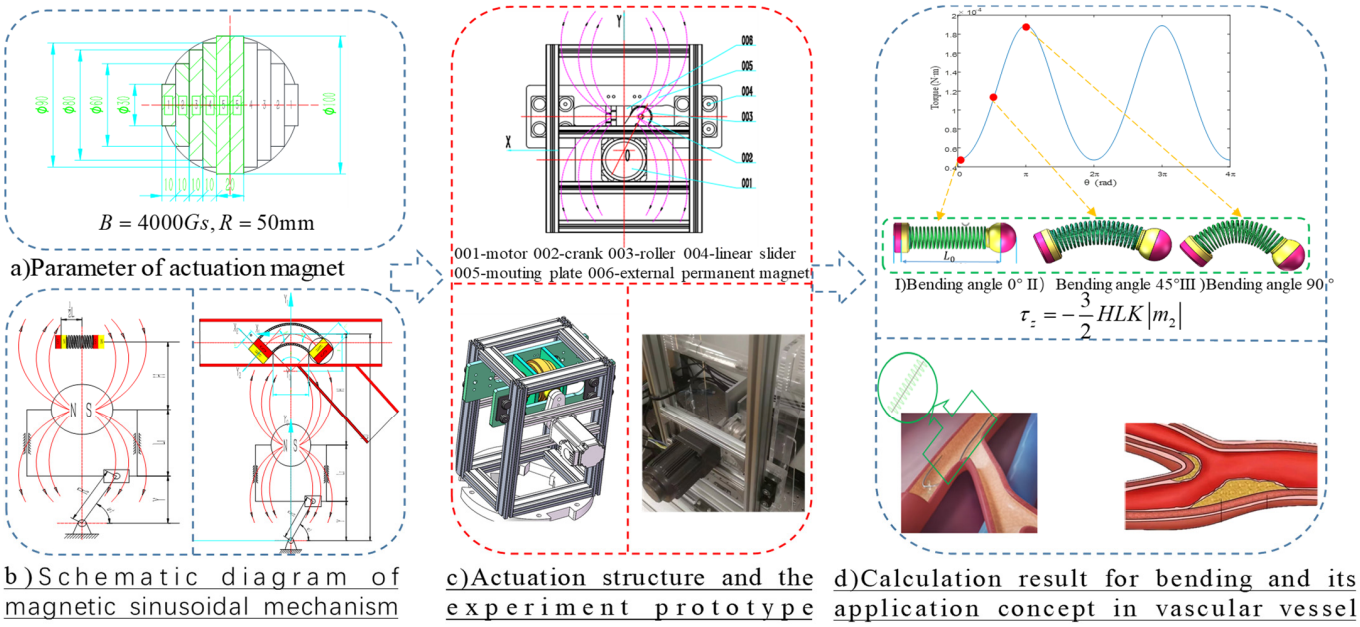


Figure 5. Magnetic sinusoidal mechanism: actuation spherical magnet, sinusoidal mechanism, and calculation outcome for bio-inspired robot.

The Euler–Bernoulli theory [28] provides a framework for calculating the relationship between the deflection angle (θ) and deflection distance δ of a spring-tube linkage.

$$M(x) = EI\frac{d^2\delta}{dx^2},\ \theta(x) = \frac{d\delta}{dx}$$

where M(x) is the actuation bending torque, E and I are Young's modulus and second moment of inertia for the tube, respectively. The bending torque varies sinusoidally with the distance between the actuation magnet and the robot, reaching a maximum of 1.9×10^{-4} N.m. Resonance can be achieved by exciting the system at a specific oscillating frequency. As the frequency of the magnetic field increases, the amplitude of the MSCR's oscillation correspondingly increases until it reaches saturation. As depicted in Figure 5d, the magnetic sinusoidal mechanism induces a harmonic response in the MSCRs, enabling the guidewire to vibrate and potentially inhibit prolapse.

3. Kirigami Skin and Friction Test

The kirigami skin is fabricated by laser cutting (10% intensity) in 0.25 mm thick PET plastic sheets (Young's modulus E = 4.11 GPa) and subsequently wrapped around the bio-inspired robot design. Upon periodic magnetic bending, the deformation of the guidewires or catheter generates a mechanical force or torque within the kirigami skin, which in turn elicits a three-dimensional (3D) morphology resembling that of a cutting balloon's edge for a better drug absorption rate, as depicted in Figure 6.

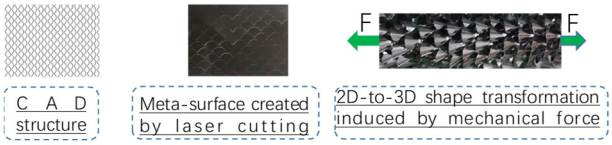


Figure 6. Fabrication procedure of kirigami skin by CAD design and 2D-3D transformation.

An array of arches with circumferential angles measured at 60 degrees has been designed using Computer-Aided Design (CAD) software(2016). This pattern can be replicated through laser cutting in PET membrane, and a 2D-to-3D shape transformation can be induced by mechanical force, as illustrated in Figure 6. This demonstrates the ability to modulate the frictional properties of the guidewire, thereby facilitating precise manipulation and enabling the establishment of proximal anchoring points, which are crucial for guiding wire direction selection or performing electrophysiological procedures such as the radiofrequency (RF) ablation of cardiac arrhythmias. The 2D-to-3D shape-morphing process induced by the kirigami skin mimics the snakes' capacity to actively manipulate their scales (as shown in Movie S1), enabling the tuning of frictional properties.

As shown in Figure 7, the designed kirigami is adhered to the outside of the MSCRs and has been proven to dynamically enhance frictional properties, acting as an anchor point with the potential to inhibit buckling during vascular interventional surgery, similar to a cutting balloon.

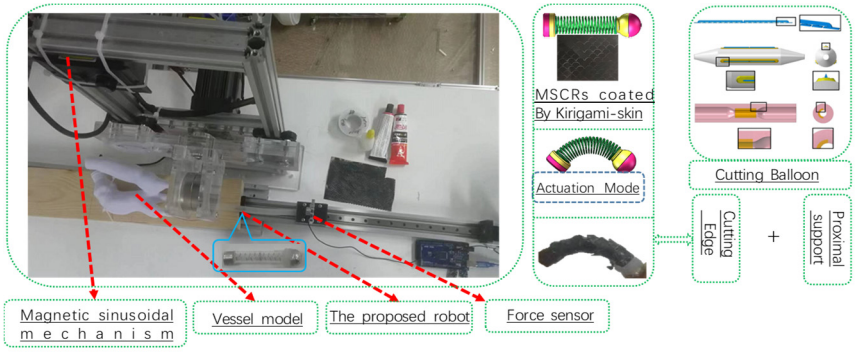


Figure 7. An experimental platform was developed for the precise measurement of the frictional properties of our kirigami-skin micro-robot.

4. Actuation in MSCRs

Actuation is accomplished through the manipulation of an external magnet using a serial manipulator. This manipulation results in the generation of force and torque on an internal magnet embedded within the guidewire or catheter. The navigation robot is developed utilizing a dual-parallelogram mechanical structure, which is characterized by its ability to independently manipulate both the magnetic navigation direction and density [29]. This design feature facilitates improved magnetic navigation capabilities.

As illustrated in Figure 8, a dual-parallelogram structure consists of two parallelogram linkages arranged in parallel. Each parallelogram linkage is formed by four links connected by revolute joints, with two of the links being parallel to each other. The primary function of this configuration is to maintain the orientation of the end effector or

a moving platform, ensuring that it rotates about a virtual axis. The slider linear axis passes though the virtual point, and the navigation robot with the VCM point has been designed to actively change the orientation of the guidewire. During the actuation and rotation of the robot, a synchronous magnetic field with constant strength is generated at the VCM point, which is intuitively utilized to control the orientation of the MSCRs through magnetic interaction. Magnetic distribution and density have been analyzed by FEA for better system performance.

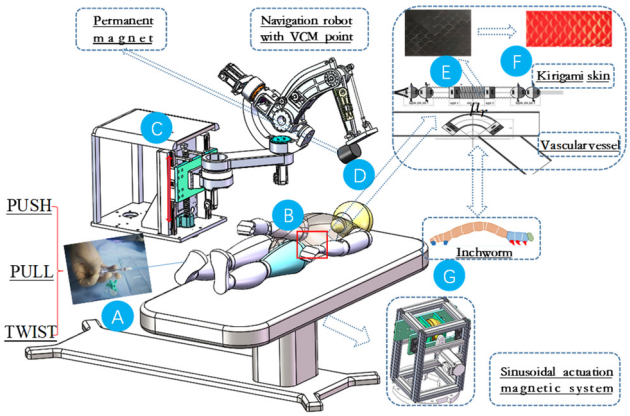


Figure 8. A novel magnetic navigation system for vascular interventions involves surgeon A inserting a magnetic guidewire into patient B. A semi-autonomous navigation robot C precisely positions a permanent magnet D within the workspace to guide the guidewire. The proposed guidewire E exhibits a motion gait analogous to an inchworm equipped with kirigami skin F, which is actuated by a sinusoidal magnetic mechanism G.

Compared to electromagnetic actuation (EMA) systems, permanent-magnet systems possess the capability to generate clinically relevant forces with a high strength-to-size ratio, offering cost-effectiveness and a compact form factor. A cylindrical NdFeB magnet has been designed to actuate the proposed magnetic soft continuum robots (MSCRs). The radius and height of the cylindrical magnet are denoted as R and H, respectively. The magnetic field along the axis of the cylindrical magnet can be mathematically expressed as a function of the distance from its surface (denoted as z) [30,31].

$$B_Z = \frac{B_0\sqrt{R^2+H^2}}{H}\left(\frac{z+H}{\sqrt{(z+H)^2+R^2}} - \frac{z}{\sqrt{z^2+R^2}}\right) \tag{12}$$

The surface field strength B_0 of the actuated magnet is 4000 Gs. The field gradient along the central axis of the cylindrical magnet can be calculated using Equation (12), which represents the derivative of the field strength with respect to z.

$$\frac{\partial B_Z}{\partial z} = \frac{B_0\sqrt{R^2+H^2}}{H}\left(\frac{1}{\sqrt{(z+H)^2+R^2}} - \frac{1}{\sqrt{z^2+R^2}} + \frac{z^2}{(z^2+R^2)^{3/2}} - \frac{(z+H)^2}{((z+H)^2+R^2)^{3/2}}\right) \tag{13}$$

The derivation of composite functions with respect to time t is as follows:

$$\frac{dB_Z}{dt} = \frac{\partial B_Z}{\partial z}\frac{dz}{dt}$$

where $\frac{dz}{dt}$ is the velocity of the linear slider, as indicated by Equation (8), the derivative of actuation field with respect to time is positive correlated to navigation force.

Based on the deflection model outlined in Section 2, the external permanent magnet (EPM) navigated by a dual-parallelogram mechanism is capable of adjusting the bending angle of MSCRs through either attraction or repulsion modes, as illustrated in Figure 9. The P_{WVcm} vector with a non-zero Z-component solely in a local coordinate system can be

transformed to the world coordinate system via left multiplication by the rotation matrix. The matrix $J_R(q)$, representing the Jacobian of the actuation robot, is derived using DH parameters. The dual-parallelogram structure, mounted directly on the robot, leverages axes 4 and 5. $J_R(q)$ links the wrist point velocity to the joint velocities of each axis. The joint angular velocity, along with vector P_{WVcm}, contributes an additional velocity component, as calculated by the cross-product of $\Omega \times P$. The Jacobian attached to point VCM could be expressed in the following equation.

$$J_{Vcm}(q) = \begin{bmatrix} I & -{}^0_5R^5 P_{WVcm} {}^0_5R^T \\ 0 & I \end{bmatrix} J_R(q)$$

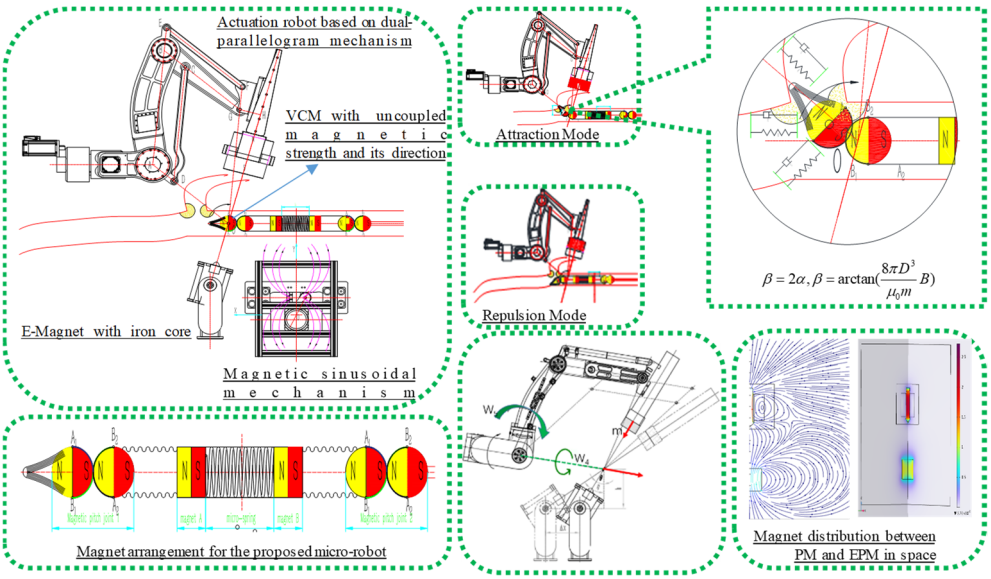


Figure 9. EPM navigation system and the magnet distribution between PM and EPM in space.

Then, the derivative of the position and magnetic moment could be expressed in the following equation.

$$\begin{bmatrix} \dot{P}_a \\ \dot{m}_a \end{bmatrix} = \begin{bmatrix} I & 0 \\ 0 & S(\widehat{m_a}) \end{bmatrix} \begin{bmatrix} I & -{}^0_5R^5 P_{WVcm} {}^0_5R^T \\ 0 & I \end{bmatrix} J_R(q)$$

This parameter could be exploited in the velocity loop for better system performance as in [32]. Additionally, to predict the deformation of MSCRs in the magnetic field, a simplified model grounded in the principle of total potential energy has been proposed to describe their deformation behavior.

$$W = W_{magnet} + W_{spring}$$
$$W_{magnet} = \int -\frac{1}{\mu_0} \vec{B_r} \vec{B} dV$$
$$W_{spring} = \frac{1}{2} k(\Delta x)^2 + M\theta$$

For the proposed MSCRs, the deflection angle can be determined by calculating the derivative of the total potential energy.

5. In Vitro Navigation of Devices in Artificial Human Vascular Models

To evaluate the proposed system and novel MSCRs, a series of experimental setups depicted in Figure 10 were constructed. The system comprises a navigation robot, a magnetic sinusoidal mechanism, and the caterpillar-inspired robot, which is fabricated using magnetic pairs. A screen has been designed to monitor the real-time movement of the

robot. All commands for these components are executed through a custom C++ program utilizing Microsoft Foundation Classes (MFCs).

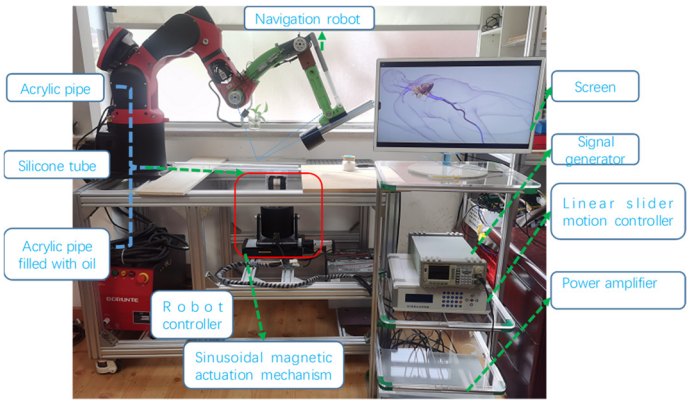


Figure 10. Experiment setup for caterpillar-inspired vascular interventional robot.

The VCM-based navigation system tests spherical magnetic chains. The sinusoidal magnetic mechanism induces a caterpillar-like locomotion gait for better maneuverability while novel MSCRs offer an optimal guidewire structure.

The stride is calculated by the following formula (as depicted by Figure 11c):

$$s = L_0 - (l_1 \cos \beta_1 + l_1 \cos \beta_2) - w$$

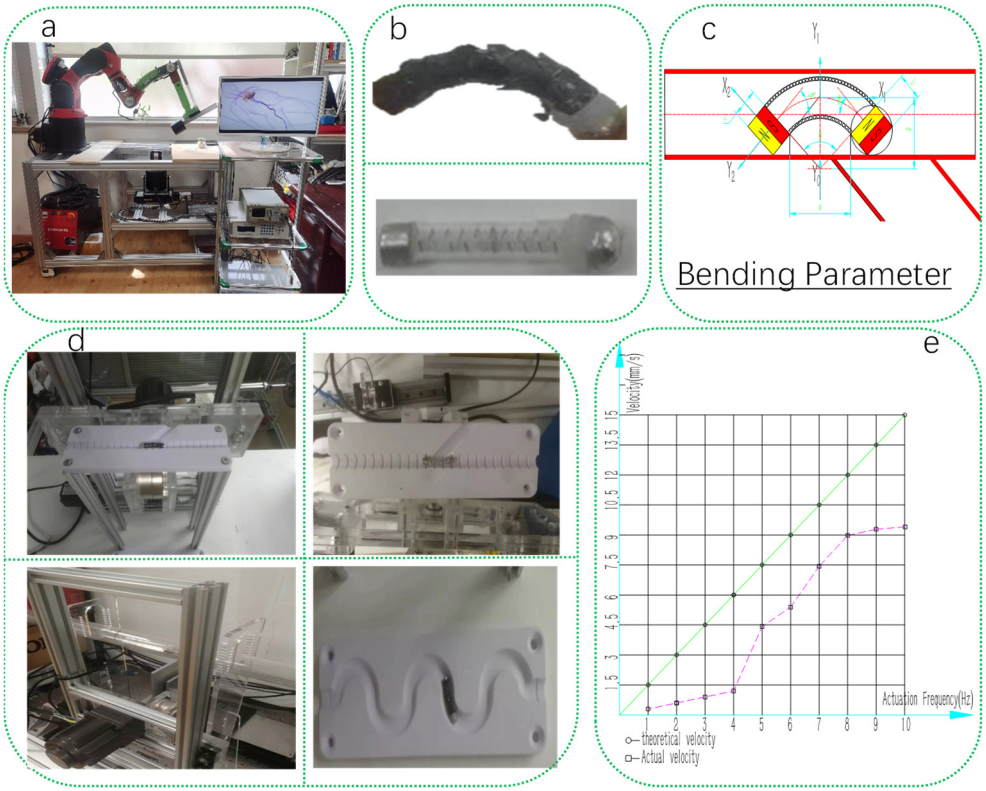


Figure 11. Experiment setup and its outcome. (**a**) the experiment setup. (**b**) Prototype of the bio-inspired soft robot. (**c**) Stride analysis geometry model. (**d**) Experiment scenarios. (**e**) Experiment outcome.

β_1 and β_2 are the maximum angles between the robot's ends and the ground during movement, with s = 1.5 for the experimental system matching FEA analysis. The theoretical

velocity scales linearly with the actuation frequency. Pipes with varying friction coefficients, including acrylic, silicone, oil-filled acrylic, and compressed air, were tested.

$$v_{theory} = s * f$$

It has been proved that the caterpillar-inspired robot moves by periodically anchoring the front end, lifting the center and pulling the rear end forward, followed by anchoring the rear end, relaxing the center and moving the front end forward to return to its flat state because of the periodic bending torque of the actuated magnet and the friction variance of the two legs. MSCRs respond poorly to low actuation frequencies (1–4 Hz). Above 5 Hz, they linearly follow the sinusoidal actuation magnet until saturation occurs at frequencies above 8 Hz (as depicted by Figure 11e).

In addition, the turning motion is controlled in conjunction with the deflection model of the diametrical magnetized spherical chain, and tortuous paths are employed to assess the performance of the innovative MSCRs. Additional tests have been conducted to evaluate the potential of MSCRs in vessel interventional surgery.

6. Discussion

We present the design of a caterpillar-inspired biomimetic catheterization robot, comprising three segments: the body, the head, and the tail feet. A cylindrical permanent magnet has been mounted on a dual-parallelogram structure, aligning its axis with the VCM point, preserving its key property. Integrating this with a spherical mini-magnet deflection system optimizes the navigation robot, offering a simplified, intuitive medical instrument. The novel navigation system, utilizing a robotically controlled magnet, allows for versatile access to the patient from various angles, eliminating the need for repositioning. Its robotic flexibility is crucial for facilitating swift fluoroscopic imaging and maneuverability in emergency scenarios.

Furthermore, a magnetic sinusoidal mechanism has been implemented to provide an efficient actuation system that mimics the anchor push–anchor pull locomotion gait of an inchworm. This approach overcomes the limitations associated with the direct pull of damping magnetic force and torque. The robot's rich shape-shifting capabilities and caterpillar-style locomotion, characterized by high displacement per actuation cycle, enable it to navigate complex pathological vessel environments. The robot has been tested successfully in various experimental tubes, including acrylic pipes, silicone tubes, and acrylic pipes filled with oil and compressed air, achieving a linear speed of 1.5 mm/s and demonstrating high locomotion efficiency. This underscores the versatility and dexterity of the developed bio-inspired magnetic micro-robot. The same micro-spring linkage connected by the micro-magnet with different magnetization directions has been analyzed for the optimal structure.

In the future, to achieve a precise and intelligent catheterization, the development of medical imaging technologies, including ultrasound (utilizing radio frequencies) and magnetic field positioning systems [31–36], will be pursued for the closed-loop control of magnetic steering and control robots (MSCRs). An integrated experimental setup, incorporating a commercial X-ray imaging system, will be employed to conduct in vivo experiments to evaluate the performance of the proposed system. Additionally, the manufacturing of next-generation miniaturized MSCRs [37] will be undertaken to pave the way for clinical application. The development and adoption of robotically assisted vascular interventional surgery, which integrates magnetic actuation with kirigami-inspired deformable structures, represent a cost-effective, flexible, and compliant approach to improve the precision, safety, and outcomes of vascular interventional surgeries. Ultimately, this advancement will contribute to the better management of cardiovascular diseases and enhance patient care.

A four-axis laser cutting machine ought to be employed for the proposed kirigami technology, with the objective of achieving miniaturization. Additionally, a potential bidirectional injection system for the proposed MSCRs may be devised in conjunction with

three-dimensional (3D) printing techniques utilizing ferromagnetic ink. Alternatively, other solutions such as the incorporation of magnetic fibers could be explored for the purpose of miniaturization. Furthermore, the proposed MSCRs have the potential to simplify certain clinical applications, such as the "Guidewire Kissing Technique".

7. Conclusions

This study explores the implementation of a magnetic sinusoidal actuation mechanism utilizing spherical magnets in the design of a bio-inspired robotic system. This mechanism harnesses the periodic displacement pattern of sinusoidal motion, driven by the magnetic interactions between the spherical magnets, to facilitate locomotion or a specific functional motion in the robotic platform. The calculation outcomes analyze the dynamic behavior, efficiency, and performance parameters of this magnetic actuation approach within the context of the bio-inspired robot's design.

Supplementary Materials: The following supporting information can be downloaded at https://www.mdpi.com/article/10.3390/act13100412/s1. Movie S1.

Author Contributions: Conceptualization, X.Z. (Xinping Zhu); methodology, X.Z. (Xinping Zhu); software, H.Z.; validation, X.Z. (Xiaoxiao Zhu); formal analysis, X.Z. (Xinping Zhu); investigation, X.Z. (Xinping Zhu); resources, K.W.; data curation, H.Z.; writing—original draft preparation, X.Z. (Xinping Zhu); writing—review and editing, X.Z. (Xiaoxiao Zhu); visualization, H.Z.; supervision, K.W.; project administration, X.Z. (Xinping Zhu); funding acquisition, K.W. All authors have read and agreed to the published version of the manuscript.

Funding: This work was supported in part by the University PH.D. Candidate Research Fund and SJTU-SAST Joint-Fund (Grand No. USCAST2023-26).

Data Availability Statement: Data is contained within the article or Supplementary Materials.

Conflicts of Interest: The authors declare no conflicts of interest.

References

1. Feigin, V.; Lawes, C.; Bennett, D.; Barker-Collo, S.; Parag, V. Worldwide stroke incidence and early case fatality reported in 56 population-based studies: A systematic review. *Lancet Neurol.* **2009**, *8*, 355. [CrossRef] [PubMed]
2. Rafii-Tari, H.; Payne, C.J.; Yang, G.-Z. Current and emerging robot-assisted endovascular catheterization technologies: A review. *Ann. Biomed. Eng.* **2014**, *42*, 697–715. [CrossRef] [PubMed]
3. Tóth, G.G.; Yamane, M.; Heyndrickx, G.R. How to select a guidewire: Technical features and key characteristics. *Heart* **2015**, *101*, 645–652. [CrossRef] [PubMed]
4. Mont'Alverne, F.J.A.; Lima, F.O.; de Araújo Rocha, F.; de Almeida Bandeira, D.; de Lucena, A.F.; Silva, H.C.; Lee, J.S.; Nogueira, R.G. Unfavorable vascular anatomy during endovascular treatment of stroke: Challenges and bailout strategies. *J. Stroke* **2020**, *22*, 185–202.
5. Loeve, A.J.; Breedveld, P.; Dankelman, J. Scopes Too Flexible. . .and Too Stiff. *IEEE Pulse* **2010**, *1*, 26. [CrossRef]
6. Grundeken, M.J.; Li, X.; Kurpershoek, C.E.; Kramer, M.C.; Vink, A.; Piek, J.J.; Tijssen, J.G.P.; Koch, K.T.; Wykrzykowska, J.J.; De Winter, R.J.; et al. Distal embolization of hydrophilic-coating material from coronary guidewires after percutaneous coronary interventions. *Circ. Cardiovasc. Interv.* **2015**, *8*, e001816. [CrossRef]
7. Pittiglio, G.; Lloyd, P.; da Veiga, T.; Onaizah, O.; Pompili, C.; Chandler, J.H.; Valdastri, P. Patient-Specific Magnetic Catheters for Atraumatic Autonomous Endoscopy. *Soft Robot.* **2022**, *9*, 1120–1133. [CrossRef]
8. Zheng, Z.; Kumar, P.; Chen, Y.; Cheng, H. Model-Based Control of Planar Piezoelectric Inchworm Soft Robot for Crawling in Constrained Environments. In Proceedings of the 2022 IEEE 5th International Conference on Soft Robotics (RoboSoft), Edinburgh, UK, 4–8 April 2022.
9. Ikuta, K.; Matsuda, Y.; Yajima, D.; Ota, Y. Precise Bending Angle Control of Hydraulic Active Catheter by Pressure Pulse Drive. In Proceedings of the 2010 IEEE International Conference on Robotics and Automation Anchorage Convention District, Anchorage, AK, USA, 3–8 May 2010.
10. Venkiteswaran, V.K.; Samaniego, L.F.; Sikorski, J.; Misra, S. Bio-Inspired Terrestrial Motion of Magnetic Soft Millirobots. *IEEE Robot. Autom. Lett.* **2019**, *4*, 1753–1759. [CrossRef]
11. Wang, W.; Lee, J.Y.; Rodrigue, H.; Song, S.H.; Chu, W.S.; Ahn, S.H. Locomotion of inchworm-inspired robot made of smart soft composite (SSC). *Bioinspir. Biomim.* **2014**, *9*, 046006. [CrossRef]
12. Stereotaxis Inc. Genesis Robotic Magnetic Navigation System with Stereotaxis Imaging Model S Fluoroscope Site Planning Considerations. 2019. Available online: https://www.roboticep.com/clinical-data/ (accessed on 22 May 2019).

13. Joyee, E.B.; Pan, Y. A Fully Three-Dimensional Printed Inchworm-Inspired Soft Robot with Magnetic Actuation. *Soft Robot.* **2019**, *6*, 333–345. [CrossRef]
14. Wu, S.; Hong, Y.; Zhao, Y.; Yin, J.; Zhu, Y. Caterpillar-inspired soft crawling robot with distributed programmable thermal actuation. *Sci. Adv.* **2023**, *9*, eadf8014. [CrossRef] [PubMed]
15. Dreyfus, R.; Boehler, Q.; Lyttle, S.; Gruber, P.; Lussi, J.; Chautems, C.; Gervasoni, S.; Berberat, J.; Seibold, D.; Ochsenbein-Kölble, N.; et al. Dexterous helical magnetic robot for improved endovascular access. *Sci. Robot.* **2024**, *9*, eadh0298. [CrossRef] [PubMed]
16. Dorfmann, A.; Trimmer, B.; Woods, W. A constitutive model for muscle properties in a soft-bodied arthropod. *J. R. Soc. Interface* **2007**, *4*, 257–269. [CrossRef] [PubMed]
17. Keller, J.B.; Falkovitz, M.S. Crawling of worms. *J. Theor. Biol.* **1983**, *104*, 417–442. [CrossRef]
18. Ghanbari, A.; Rostami, A.; Noorani, S.M.R.S.; Fakhrabadi, M.M.S. Modeling and simulation of inchworm mode locomotion. In Proceedings of the Intelligent Robotics and Applications: First International Conference, ICIRA 2008, Wuhan, China, 15–17 October 2008; pp. 617–624.
19. Rafsanjani, A.; Zhang, Y.; Liu, B.; Rubinstein, S.M.; Bertoldi, K. Kirigami skins make a simple soft actuator crawl. *Sci. Robot.* **2018**, *3*, eaar7555. [CrossRef]
20. Babaee, S.; Shi, Y.; Abbasalizadeh, S.; Tamang, S.; Hess, K.; Collins, J.E.; Ishida, K.; Lopes, A.; Williams, M.; Albaghdadi, M.; et al. Kirigami-inspired stents for sustained local delivery of therapeutics. *Nat. Mater.* **2021**, *20*, 1085–1092. [CrossRef]
21. Jeon, S.; Hoshiar, A.K.; Kim, K.; Lee, S.; Kim, E.; Lee, S.; Kim, J.-Y.; Nelson, B.J.; Cha, H.-J.; Yi, B.-J.; et al. A magnetically controlled soft micro-robot steering a guidewire in a three dimensional phantom vascular network. *Soft Robot.* **2019**, *6*, 54–68. [CrossRef]
22. Back, J.; Lindenroth, L.; Rhode, K.; Liu, H. Model-free position control for cardiac ablation catheter steering using electromagnetic position tracking and tension feedback. *Front. Robot. AI* **2017**, *4*, 17. [CrossRef]
23. Settecase, F.; Sussman, M.S.; Wilson, M.W.; Hetts, S.; Arenson, R.L.; Malba, V.; Bernhardt, A.F.; Kucharczyk, W.; Roberts, T.P.L. Magnetically-assisted remote control (MARC) steering of endovascular catheters for interventional MRI: A model for deflection and design implications. *Med. Phys.* **2007**, *34*, 3135. [CrossRef]
24. O'Donoghue, K.; Cantillon-Murphy, P. Deflection modeling of permanent magnet spherical chains in the presence of external magnetic fields. *J. Magn. Magn. Mater.* **2013**, *343*, 251–256. [CrossRef]
25. Pantula, A.; Datta, B.; Shi, Y.; Wang, M.; Liu, J.; Deng, S.; Cowan, N.J.; Nguyen, T.D.; Gracias, D.H. Untethered unidirectionally crawling gels driven by an asymmetry in contact forces. *Sci. Robot.* **2022**, *7*, eadd2903. [CrossRef] [PubMed]
26. Abbott, J.J.; Diller, E.; Petruska, A.J. Magnetic Methods in Robotics. *Annu. Rev. Control Robot. Auton. Syst.* **2020**, *3*, 57–90. [CrossRef]
27. Kratochvil, B.E.; Frutiger, D.; Vollmers, K.; Nelson, B.J. Visual Servoing and Characterization of Resonant Magnetic Actuators for Decoupled Locomotion of Multiple Untethered Mobile Microrobots. In Proceedings of the IEEE International Conference on Robotics and Automation, Kobe, Japan, 12–17 May 2009.
28. Katz, S.; Givli, S. The post-buckling behavior of a beam constrained by springy walls. *J. Mech. Phys. Solids* **2015**, *78*, 443–466. [CrossRef]
29. Zhang, W.; Meng, Y.; Huang, P. A Novel Method of Arraying Permanent Magnets Circumferentially to Generate a Rotation Magnetic Field. *IEEE Trans. Magn.* **2008**, *44*, 2367–2372. [CrossRef]
30. Kim, Y.; Parada, G.A.; Liu, S.; Zhao, X. Ferromagnetic soft continuum robots. *Sci. Robot.* **2019**, *4*, eaax7329. [CrossRef]
31. Kim, Y.; Genevriere, E.; Harker, P.; Choe, J.; Balicki, M.; Regenhardt, R.W.; Vranic, J.E.; Dmytriw, A.A.; Patel, A.B.; Zhao, X. Tele-robotic neurovascular interventions with magnetic manipulation. *Sci. Robot.* **2022**, *7*, eabg9907. [CrossRef]
32. Heunis, C.M.; Silva, B.; Sereni, G.; Lam, M.C.; Belakhal, B.; Gaborit, A.; Wermelink, B.; Geelkerken, B.R.; Misra, S. The Flux One Magnetic Navigation System: A Preliminary Assessment for Stent Implantation. *IEEE Robot. Autom. Lett.* **2023**, *8*, 5640–5647. [CrossRef]
33. Wang, Q.; Chan, K.F.; Schweizer, K.; Du, X.; Zhang, L. Ultrasound doppler-guided real-time navigation of a magnetic microswarm for active endovascular delivery. *Sci. Adv.* **2021**, *7*, eabe5914. [CrossRef]
34. Aranda-Michel, E.; Yi, J.; Wirekoh, J.; Kumar, N.; Riviere, C.N.; Schwartzman, D.S.; Park, Y.L. Miniaturized robotic end-effector with piezoelectric actuation and fiber optic sensing for minimally invasive cardiac procedures. *IEEE Sens. J.* **2018**, *18*, 4961–4968. [CrossRef]
35. Kumar, N.; Wirekoh, J.; Saba, S.; Riviere, C.N.; Park, Y.-L. Soft miniaturized actuation and sensing units for dynamic force control of cardiac ablation catheters. *Soft Robot.* **2021**, *8*, 59–70. [CrossRef]
36. Kim, J.; Chung, S.; Choi, S.; Lee, H.; Kwon, S. Programming magnetic anisotropy in polymeric micro-actuators. *Nat. Mater.* **2011**, *10*, 747–752. [CrossRef] [PubMed]
37. Lee, Y.; Koehler, F.; Dillon, T.; Loke, G.; Kim, Y.; Marion, J.; Antonini, M.J.; Garwood, I.C.; Sahasrabudhe, A.; Nagao, K.; et al. Magnetically Actuated Fiber-Based Soft Robots. *Adv. Mater.* **2023**, *35*, 2301916. [CrossRef] [PubMed]

Disclaimer/Publisher's Note: The statements, opinions and data contained in all publications are solely those of the individual author(s) and contributor(s) and not of MDPI and/or the editor(s). MDPI and/or the editor(s) disclaim responsibility for any injury to people or property resulting from any ideas, methods, instructions or products referred to in the content.